Impact of electrolytic hydrogen charging on the mechanical properties and microstructure of AISI 304 austenitic stainless steel

Amar Abboub[a], *Ahmed* Aboura[b], *Khaled* Benmahdi[c], *Mohamed* Sadoun[d], *Mohamed* Boukhelef[e]

[a] Mustapha Stambouli University, Faculty of Sciences and Technology, Department of Mechanical Engineering, Mascara, People's Democratic Republic of Algeria, e-mail: abboub.amar@yahoo.com, **corresponding author**, ORCID iD: https://orcid.org/0009-0004-0158-5837

[b] Ahmed Zabana University, Faculty of Sciences and Technology, Department of Mechanical Engineering, Relizane, People's Democratic Republic of Algeria, e-mail: ahmed.aboura@univ-relizane.dz, ORCID iD: https://orcid.org/0009-0005-3509-2026

[c] Mustapha Stambouli University, Faculty of Sciences and Technology, Department of Civil Engineering, Laboratory for the Study of Structures and Mechanics of Materials, Mascara, People's Democratic Republic of Algeria, e-mail: k.benmahdi@univ-mascara.dz, ORCID iD: https://orcid.org/0000-0002-8244-5817

[d] Mustapha Stambouli University, Faculty of Sciences and Technology, Department of Civil Engineering, Laboratory for the Study of Structures and Mechanics of Materials, Mascara, People's Democratic Republic of Algeria, e-mail: m.sadoun@univ-mascara.dz, ORCID iD: https://orcid.org/0009-0008-2314-9402

[e] Mustapha Stambouli University, Faculty of Sciences and Technology, Department of Mechanical Engineering, Mascara, People's Democratic Republic of Algeria, e-mail: mohamed.boukhelef@univ-mascara.dz, ORCID iD: https://orcid.org/0009-0003-1897-9536

https://doi.org/10.5937/vojtehg73-56087

FIELD: materials
ARTICLE TYPE: original scientific paper

Abstract:

Introduction/purpose: Hydrogen embrittlement (HE) substantially decreases the mechanical properties of austenitic stainless steels, constraining their efficacy in diverse applications. This study examines the impact of electrolytic hydrogen charging on the mechanical characteristics and microstructure of AISI304 stainless steel, a commonly utilized grade.

Methods: Tensile specimens measuring 8 mm in diameter were produced through machining and subjected to hydrogen loading electrolytically at different times in a glass chamber containing sulfuric acid (H_2SO_4) at 0.05M. The mechanical tests were conducted using a Karl Frank GMBH tensile testing universal machine, type 83431. The samples underwent microscopic analysis by means of optical microscopy (OM), X-ray diffraction (XRD), and scanning electron microscopy (SEM). The experimental characterization involved producing cylindrical specimens which underwent heat treatments (austenization) ranging from quenching to tempering, followed by immersion in a cold heat treatment cycle at -196°C for 35 minutes. Hydrogen preloading was carried out through electrochemical hydrogen charged for different loading times in hours.

Results: The results showed that the effects of hydrogen embrittlement (HE) on AISI304 stainless steel are characterized by a decrease in ductility, sometimes undergoing sudden embrittlement. This phenomenon is consistently recognized by other authors who have demonstrated a loss of ductility due to the martensitic transformation of austenite caused by deformation and hydrogen diffusion.

Conclusion: Inclusions such as second-phase particles, carbide precipitates, inclusions of small, medium, or large size, interfaces, and interphases, can be considered inclusions. Their mechanical properties and hydrogen transport and segregation mechanisms differ from those of the matrix, particularly in martensitic structures. The observation of the optical dark area (ODA) and black spots indicates that hydrogen is concentrated either in the molecular form H_2 or combined with sulphur in the form of H_2S.

Key words: AISI304 stainless steel, heat treatment, mechanical properties, hydrogen charged, hydrogen embrittlement, microstructure

Introduction

Hydrogen embrittlement (HE) substantially decreases the mechanical properties of austenitic stainless steels, constraining their efficacy in diverse applications (Cauwels et al., 2019; Amar Abboub et al., 2024). This study examines the impact of electrolytic hydrogen charging on the mechanical characteristics and microstructure of AISI304 stainless steel, a commonly utilized grade. Austenitic stainless steels, especially AISI304, are extensively utilized across several industries owing to their superior mechanical qualities, corrosion resistance, and high ductility. These characteristics render them suitable for use in demanding environments, including chemical, petrochemical, and nuclear sectors. The performance of AISI304 stainless steel can be substantially compromised by hydrogen embrittlement, a significant concern for materials subjected to hydrogen-rich environments.

Chrome nickel stainless steels are steels with excellent corrosion resistance which allows them to be chosen as a material intended for application in the energy industry (Cunat, 2000; Colombié, 2008). During their operations, often in aggressive hydrogenated environments, these steels undergo degradation of their mechanical strength and ductility - this is the phenomenon of hydrogen embrittlement called the (HE) phenomenon (Brass et al., 2000). Hydrogen, diffusing in atomic (H) or molecular H_2 form in the crystal lattice of the metallic material, weakens the atomic bonds (Lynch, 2012), which results macroscopically in a change in the mechanical properties and premature cracking at a stress below the elastic limit and by the loss of ductility during mechanical stresses (Frappart et al., 2011; Creus, 2013.; Chêne, 2009). Generally, the sensitivity of stainless steels to the (HE) phenomenon is influenced by their microstructure (Brass et al., 2000; Frappart et al., 2011; Lynch, 2012). The ferritic (α) phase of iron has a hydrogen conduction coefficient greater than that of the austenitic (γ) phase; for the case of solubility, it is the opposite - the austenitic (γ) phase has a higher hydrogen solubility than that of the ferritic (α) phase (Brass et al., 2000; Chêne, 2009).

The mechanisms of hydrogen embritllement (HE) are influenced by several factors, including the materials involved and specific experimental conditions (Grimault et al., 2012; Bach, 2018; Blanchard et al., 1960; El Hilali et al., 1999; Ly, 2009; Hamissi et al., 2016; Iacoviello, 1995; Sales, 2015) such as temperature, loading speed, hydrogen content, and duration of loading (Brass et al., 2000; Chêne, 2009). Numerous studies have established that hydrogen poses a significant risk to the mechanical properties of metallic materials, particularly affecting ductility, toughness, and strength (He et al., 1999; Depover et al., 2014; Laureys et al., 2018; Cauwels et al., 2019; Robertson et al., 2015). This phenomenon is primarily linked to the interaction between existing defects in the metal and hydrogen (Brass et al., 2000; Chêne, 2009; Lynch, 2012). Research has identified various mechanisms, including the rapid diffusion of hydrogen and its quick adsorption on defects (Chêne, 2009), which adversely impact material performance. The key interactions of hydrogen with intrinsic trapping sites, such as dislocations, micro-voids, pores, grain boundaries, inclusions, and oxide-matrix interfaces (Lee & Lee, 1987; He et al., 1999; Jin et al., 2010; Murakami et al., 2013, Laureys et al., 2018), are the critical factors contributing to the degradation of mechanical characteristics. These detrimental effects are especially pronounced during mechanical tensile fracture tests (Depover et al., 2014), where the presence of hydrogen can lead to a substantial reduction in material performance. The X-ray analysis of hydrogen-loaded material revealed a pseudo-martensitic

transformation, which accounts for the observed loss of ductility in the material. Scanning electron microscope (SEM) observations indicated that hydrogen interacts with non-metallic inclusions (Murakami et al., 2013), manifesting as dark areas, referred to as observation of the optic dark area (ODA). The experimental work was essential in elucidating the hydrogen embrittlement (HE) phenomenon and its impact on the mechanical properties of the material. The study utilized AISI304 stainless steel which was an electrochemically-hydrogen preloaded process at room temperature, as referenced in multiple studies (Murakami & Matsunaga, 2006; Robertson et al., 2015; Aurélie Laureys et al., 2020; El Hilali et al., 1999; Hamissi et al., 2016; Amar, 2023).

This research work focused on studying the influence of quenching and tempering heat treatments on the (HE) phenomenon, and utilized various observation techniques including optical microscopy and scanning electron microscopy.

Experimental work

Materials

Chemical composition

The material used in this experimental study is AISI304 austenitic stainless steel with the chemical composition given in Table 1 below.

Table 1 – Chemical composition (Wt. %) of the AISI304 steel studied

Chemical composition (Wt. %)					
Fe%	C%	Cr%	Ni%	Si%	Mn%
69.35	0.0632	17.98	9.64	0.0114	1.65
P%	S%	NB%	Mo%	Al%	Co%
<0,00030	0.028	0.0491	0.365	0.0074	0.0991
B%	V%	Ti%	Cu%	W%	Pb%
0.0152	0.0864	0.0052	0.174	0.0316	0.0045

Specimen geometry

The experimental part involves using standardised DIN50125 tensile specimens with the cylindrical shape and dimensions shown in Figure 1. These specimens are machined on a semi-automatic lathe TRENS, a.s. Suvoz 91132 Slovakia, type EN 50 C.

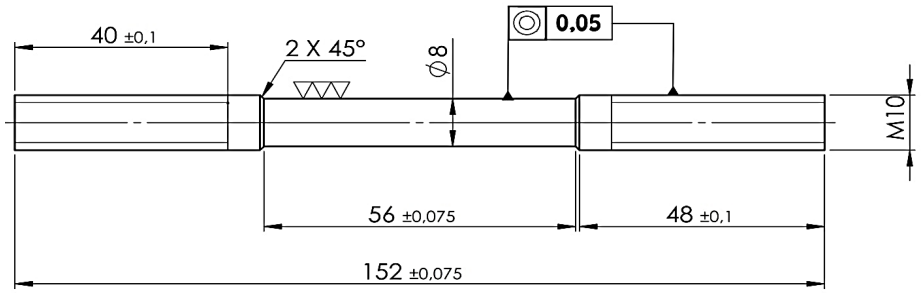

Figure 1 – Dimensions of the tensile specimens according to the standard (DIN TASCHENBUCH 19, 1975) (all dimensions are in mm)

Mechanical properties

The initial mechanical properties of the material in its raw state without heat treatment (as-delivered condition) are shown in Table 2 below.

Table 2 – Initial mechanical characteristics of the AISI304 steel

Initial mechanical properties							
Material	Rm, [TS], (Air) (MPa)	Re, [YS], (Air) (MPa)	Rr, [FS], (Air) (MPa)	A, (Air) (%)	Z, (Air) (%)	E (MPa)	υ
AISI304 As-delivered condition	686±7.03	589±1.79	414±0.12	78.5	41.5	200 000	0.27

Heat treatments

Following the fabrication of the specimens, an austenizing procedure was performed using the thermal cycle shown in Figure 2. It involves heating at 1050°C for 30 minutes and then quenching in the water.

Step two was to apply a temperature of 700°C for 35 minutes, then cool the specimens at room temperature to obtain a homogeneous and stable austenite structure. This results in a relaxation of residual stresses and an increase in the mechanical strength by micro-plasticity (BARRALIS et al., 1999; Grimault et al., 2012; Amar, 2023).

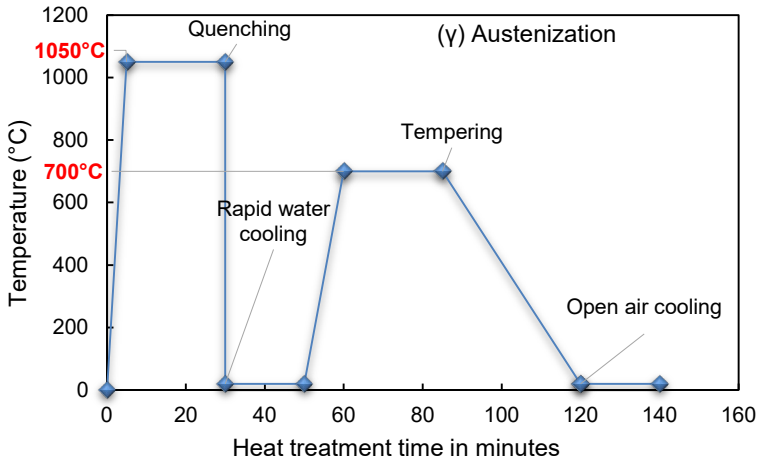

Figure 2 – Heat treatment cycle used (Amar, 2023)

Tempering at 700°C after solution quenching has several important objectives. Firstly, it aims to stabilise the austenitic microstructure by reducing the residual internal stresses caused by rapid quenching, which could otherwise promote martensite formation on subsequent stressing. Secondly, although treatment at this temperature can lead to sensitisation, particularly in AISI304 steel, a controlled short holding time at 700°C can maximise the stress stabilisation effect while minimising the risk of chromium carbide precipitation at grain boundaries, which could compromise intergranular corrosion resistance. Finally, this tempering also helps to reduce the density of residual crystalline defects. The main challenge is therefore to strike a balance between stabilising the austenite and maintaining good corrosion resistance.

Cryogenic heat treatment at -196°C

After austenitization, the tensile specimens underwent cold quenching (with N_2 liquid nitrogen bubbling) (El Hilali et al., 1999) following the thermal cycle illustrated in Figure 3 (G. Prieto et al. 2017). This type of treatment was carried out following a succession of immersions for 35 minutes and heating in the ambient air (ambient warm-up: 45 minutes). The cold quenching cycle is repeated with twenty (20) cycles.

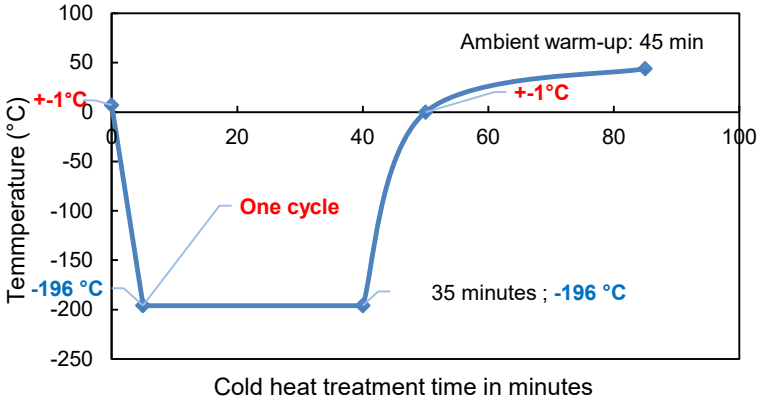

Figure 3 – Cold quenching cycle applied at -196°C (Prieto & Tuckart, 2017)

A cryogenic treatment at -196°C is presented as a method of obtaining a 'near perfect' material, based on the concept of zero entropy at 0 K. This treatment offers several potential benefits. Firstly, it can promote the transformation of residual martensite that can form as a result of internal stresses after quenching. Although a complete transformation is rare in AISI304 steel, the cryogenic treatment can contribute to this development. In addition, atomic diffusion is severely restricted at cryogenic temperatures, reducing the likelihood of significant chromium carbide formation while allowing the formation of very fine nanoprecipitates.

Cryogenic quenching can also help to reduce internal stresses through thermal cycling, which can relieve microscopic stresses. However, it is important to note that it can paradoxically increase the density of dislocations due to thermal shocks and induced stresses. These dislocations, although more numerous, could have different characteristics from those generated by machining, thus affecting hydrogen trapping. Finally, the cryogenic treatment could improve microstructural homogeneity by inducing very fine transformations or precipitates, thus contributing to a more uniform microstructure.

Conditions of electrochemically-hydrogen charged specimens

After the cyclic treatment, the specimens are electrolytically pre-charged with hydrogen. The method consists of using an enclosure containing a 0.05M (H_2SO_4) aqueous solution of sulfuric acid equipped with two electrodes, an unattackable platinum anode and a cathode connected to

the specimen, as illustrated in Figure 4 (a) and (b). Charging was carried out at room temperature with a current density equal to 100 mA/cm^2 for different durations, similarly to the author's work (Depover et al., 2014; Aurélie Laureys et al., 2020; Cauwels et al., 2019; Hamissi et al., 2016; Amar, 2023).

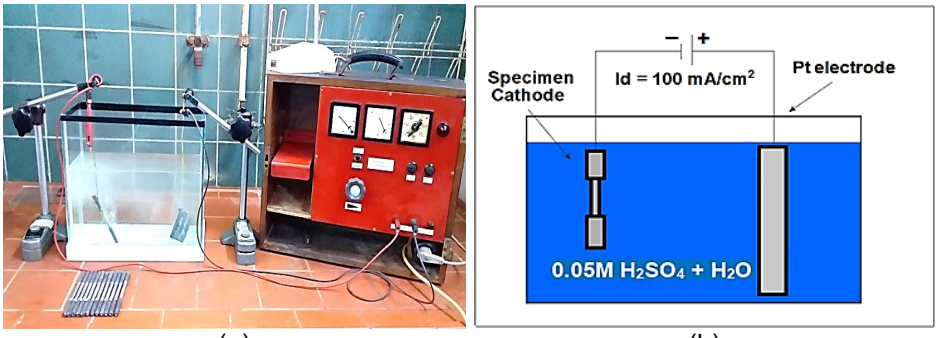

(a) (b)

Figure 4 – (a) Hydrogen-loaded specimens in 0.05M (H_2SO_4) (pH=1.32) and (b) schematic of the experimental cathodic hydrogen charging (Depover et al., 2014)

Mechanical tensile test

This experimental section describes the use of a universal (tension/compression) testing machine manufactured by Frank Karl GMBH to perform mechanical fracture tests on specimens preloaded with hydrogen. The tests were performed at a displacement speed of 20 mm/min, chosen according to the calibration of the laboratory machine. This equipment has an accuracy criterion of class 0.5, with a total measurement uncertainty of between 0.1% and 0.25%. These specifications correspond to those on the machine's nameplate and comply with DIN 50125 (DIN TASCHENBUCH 19, 1975).

Immediately after the loading process, the samples were characterized mechanically at room temperature using a tensile testing machine supplied by Karl Frank GMBH (He et al., 1999; Hamissi et al., 2016) with a maximum load capacity of 400 kN and a nominal speed of (ἑ= 20 mm/min) equipped with a table to plot experimental tensile curves (stress/strain), in order to calculate the different mechanical properties and study the hydrogen embrittlement (HE) of the steel studied, presented in Figure 5 (a), (b), and (c) and described in detail in Table 3.

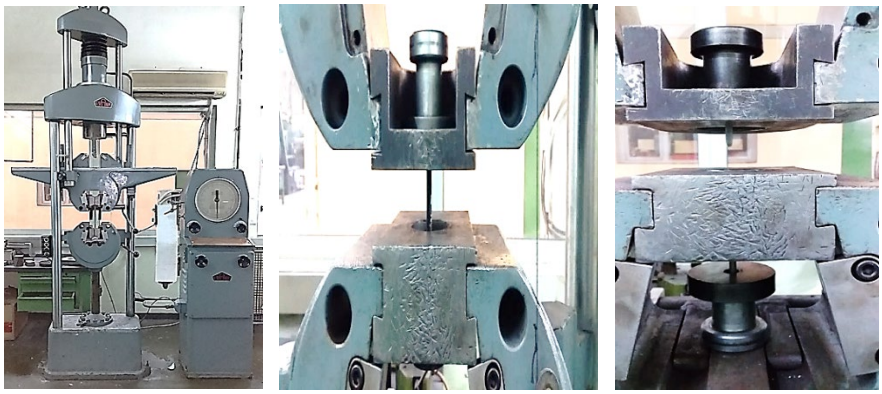

(a) (b) (c)

Figure 5 – Tensile machine Karl Frank GMBH used: (a) universal testing machine, (b) the specimen before tensile fracture, and (c) the specimen after tensile fracture (Amar, 2023)

Results and discussions

Mechanical properties

Table 3 presents the data results of the mechanical properties after the preloading protocol and the mechanical test by low tensile fracture at room temperature.

The data results of the mechanical tensile tests obtained are shown as experimental curves in Figures 6, 7, and 8 below.

The analysis of these curves shows a slight decrease in the resistance of the material as a function of the quantity of absorbed hydrogen represented by the loading duration, as Figure 6 shows. This is in agreement with the work carried out by various researchers who stipulate that hydrogen, by diffusing in the atomic form in the material, regroups in the form of (H_2) gas to occupy the existing defects and consequently exerts internal pressures (Murakami & Matsunaga, 2006), which reduces resistance (Hamissi et al., 2016). Firstly, Subfigure 6 (a) represents a decrease sensitive to the values of the mechanical resistance stress strength (Rm) as a function of hydrogen pre-charging time in hours. In parallel, a comparison of these values with the reference sample which presents a significant value is greater ($Rm_{(Air)} > Rm_{(H)}$) of the order of $Rm_{(Air)}$: 686±7.03 MPa to $Rm_{(H)}$: 532±4.44 MPa or the mechanical resistance passes through a minimum value of the order of $Rm_{(H)}$: 515±5.25 MPa, see Table 3. Secondly, a behavior expected by a yield strength (Re) in (MPa) as a function of the level of number of hours of

hydrogen preloaded, which represents a progressive reduction at this yield compared to the initial $Re_{(Air),}$ is of the order of $Re_{(Air)}$: 589±1.79 MPa to $Re_{(H)}$: 286±6.24 MPa, up to the duration of 13hours or this yield strength passes through less significant values of the order of $Re_{(H)}$: 191±9.82 MPa, as Subfigure 6 (b) shows. According to the two parameters of the variation of the mechanical resistance, stress strength $Rm_{(H)}$ and yield strength $Re_{(H)}$ in (MPa) undergo drops and progressive reductions compared to the initial $Re_{(Air)}$ value.

Table 3 – Mechanical characteristics of AISI304 after electrochemically-hydrogen preloading

Data results of tensile strength after preloading of hydrogen							
N° Specimens	Hydrogen Loaded	Stress strength, [TS]	Yield strength, [YS]	Failure strength, [FR]	Elongation percentage	Reduction percentage	Hardness (N/mm^2)
	in (hours)	Rm, MPa	Re, MPa	Rr, MPa	A, %	Z, %	$HRV_{(30)}$
As-delivered	Uncharged	686±7.03	589±1.79	414±1.12	41.5	78.8	227
Specimen.1	1 hour	532±4.44	286±6.24	302±5.47	58.2	79.7	166
Specimen.2	2 hours	553±3.43	254±7.77	334±3.94	57.7	78.6	172
Specimen.3	3 hours	553±3.43	246±8.15	336±2.42	56.5	79.7	172
Specimen.4	4 hours	549±3.63	238±8.63	350±3.18	61.3	81.9	171
Specimen.5	5 hours	541±4.01	238±8.53	342±3.56	58.2	80.8	168
Specimen.6	6 hours	551±0.24	238±8.53	358±2.80	59.6	80.8	172
Specimen.7	7 hours	545±3.82	230±8.91	358±2.80	57.9	80.8	170
Specimen.8	8 hours	551±3.53	238±8.53	350±2.80	58	80.8	172
Specimen.9	9 hours	541±4.01	230±8.91	358±2.80	57.8	80.8	166
Specimen.10	10 hours	543±3.91	230±8.91	334±3.94	69.4	82.9	169
Specimen.11	11 hours	525±4.77	230±8.91	350±3.18	57.1	80.8	165
Specimen.12	12 hours	515±5.25	222±9.29	342±6.60	64.5	81.9	158
Specimen.13	13 hours	515±5.25	191±9.82	350±3.18	57.8	80.8	158

The result is that this type of AISI304 steel studied is fragile under the effect of the industrial conditions adopted (Robertson et al., 2015; Cauwels et al., 2019) and in tests in the presence of the aggressive environment, the solution used is (H_2SO_4) acid at 0.05M with nitrogen bubbling (El Hilali et al., 1999) and different loading times in hours. Thus the value of the density of the applied polarization is 100 mA/cm^2 in order to carry the internal microcracks induced by the influence of these mechanical properties due to the absorption of charged hydrogen, as Subfigure 9 (b) shows. The yield strength (Re) and the failure strength (Rr) decrease, as

Figure 6 shows, with the increase in the tempering temperature due to the mobility and movement of carbon atoms towards preferential sites, the decrease in carbon concentration in the martensite quenched due to the diffusion of carbon atoms in cementite, and the decrease in dislocation density and lowering of hardening (Bhadeshia & Honeycombe, 2006).

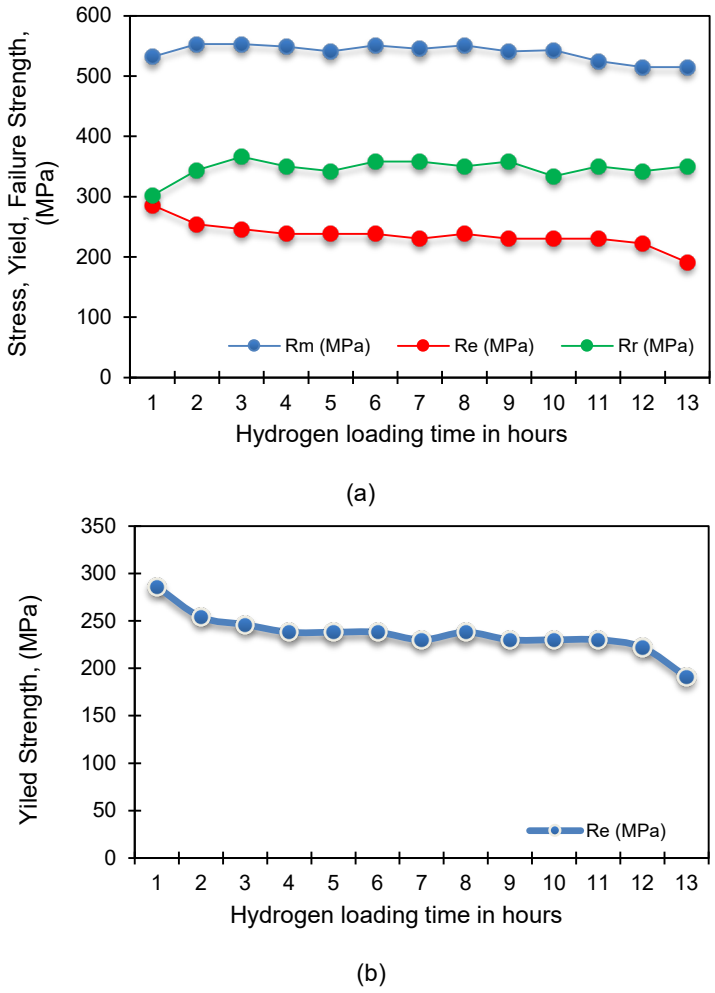

Figure 6 – (a) Variation of the resistance of stress strength, Rm, yield strength, Re and failure strength, Rr, and (b) the yield strength of AISI304 steel with loading duration in hydrogen medium sulfuric acid (H_2SO_4)

Plasticity variation

Figure 7 shows the variation of the plasticity properties for the steel studies, which is improved by the hydrogen preloading conditions in order to undergo a light increase in percentage reduction Z (%) compared to the reference $Z_{(Air)}$ (78.5 %) to $Z_{(H)}$ (79.7 %) in order to reach a value that becomes stable throughout the level in hours, which is $Z_{(H)}$ - 80.8 %. This leads to a variation in the percentage elongation A (%) , which increases relative to the reference condition from $A_{(Air)}$ - 41.5 % to $A_{(H)}$ - 58.2 % until it stabilizes at a plasticity value of $A_{(H)}$ of 57.8 %, as Table 3 shows. We also note that, in general, the variation in the plasticity values of the ($Z\%_{(Air)} < Z\%_{(H)}$), ($A\%_{(Air)} < A\%_{(H)}$) steel studied at the maxima increases significantly and remains almost constant throughout the hydrogen time loading stage in hours due to the duration and the sets of heat treatments of tempering at 700°C (El Hilali et al., 1999) and thus the use of the protocol immersion in succession following the cycle applied by cold quenching at -196°C (Prieto & Tuckart, 2017; Amar, 2023).

The experimental results obtained show that the plasticity indicators, ZH% and AH%, increase in the presence of hydrogen compared to the unloaded specimen, Z(Air)%, A(Air)%, in its delivery state and without heat treatment. This increase is directly correlated to the maximum number of dips during cryogenic quenching cycles at -196°C. Furthermore, this observed improvement in the plasticity indicators is attributed to the initial grain refinement, similarly to the results in the work (G. Prieto & Tuckart., 2017), which contributes to reduce the surface porosity of the studied AISI304 steel.

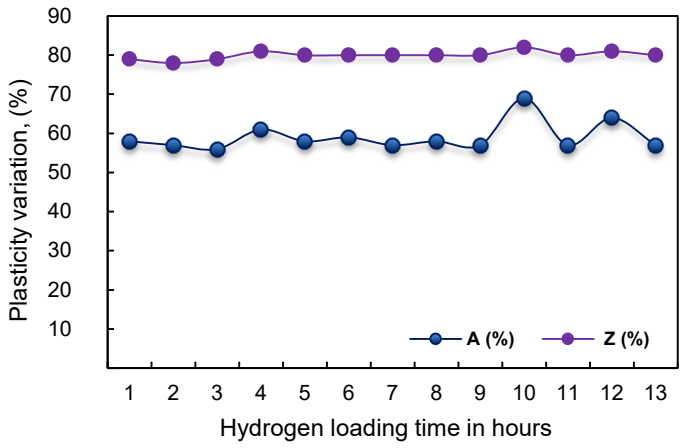

Figure 7 – Plasticity variation against hydrogen loading time

Hardness

Figure 8 shows the results of the evolution of hardness which undergoes a change in the level of loading time in hours. We noticed ($HRV_{(Air)} > HRV_{(H)}$) that the reference specimen presents the greatest value in $HRV_{(Air)}$ of the order of 227 N/mm^2 in relation to other test specimens which are pre-loaded during different hydrogen cathodic charging times of the order of $HRV_{(H)}$ of 166 N/mm^2. Where the hardness passes through a minimum value, HRV hardness ($HRV_{(H)}$) is of the order of 158 N/mm^2, as Table 3 shows.

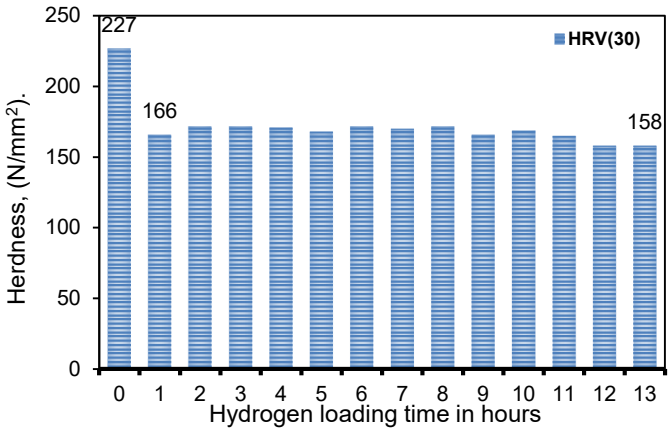

Figure 8 – Evolution hardness HRV versus hydrogen loading time

The AISI304 austenitic steel (quenched/tempered) possesses a martensitic structure after the previous heat treatments. Its structure can be embrittled by hydrogen (HE), which may manifest as transgranular facies characterized by an initiation site (inclusions) known as "fish eye". This type of defect can be highlighted during mechanical stress through tensile fracture tests. The results in a decrease in elongation at fractures and necking are shown in Subfigure 9 (b). It is a consequence of hydrogen enrichment at inclusions, grain boundaries, and micro-cavities, as well as carbide precipitations (trapping). These interfaces can be embrittled in the presence of hydrogen due to an inclusionary state, a precipitation state, segregation of chemical species, and residual austenite.

States of specimen faces

The study investigates the microstructure and fracture characteristics of AISI304 steel through various mechanical tests. Tensile tests conducted

in the air serve as a baseline, revealing the specimen crude state without any heat treatments, as Subfigure 9 (a) shows. In contrast, the tests performed in the hydrogen environment for 13 hours, following quenching at 1050°C and tempering at 700°C, show significant internal cracking along the edges of the cylindrical specimen (Subfigure 9 (b)) (Aurélie Laureys et al., 2020). This damage is attributed to a high concentration of absorbed hydrogen which adversely affects the matrix integrity under industrial conditions. The findings highlight the detrimental impact of hydrogen exposure on the mechanical properties of AISI304 steel. The diffusion and penetration of hydrogen molecules, particularly in the form of (H_2), are more pronounced in the austenitic phase (γ) of metals compared to the ferritic phase (α), even at room temperature (Frappart et al., 2011). This phenomenon leads to a significant deterioration of the metal's mechanical properties under various mechanical stresses during application. The observations regarding AISI304 steel, which was mechanically deformed and subjected to tensile loading, reveal a heightened sensitivity to crack initiation (Subfigure 9 (b)), with numerous inclusions present on the surface of the hydrogen-loaded samples. The deformed samples show an increased concentration of dislocation tangles at the interface with the matrix, resulting in localized hydrogen accumulation that promotes crack formation. Additionally, the presence of mico-voids (Subfigure 11 (b)), further accelerates the hydrogen embrittlement mechanism. The high number of inclusions in the material (Subfigure 10 (b)), along with the initiation of cracks at the grain boundaries and near these inclusions, suggests that they may act as nucleation points for hydrogen-induced cracks.

(a) (b)

Figure 9 – Specimen faces after mechanical fracture at tensile testing: (a) crude state faces, and (b) propagation of cracking faces, after the hydrogen pre-loaded state of 13hours

This results in a localized increase in hydrogen molecule concentration at the interface of the test specimen, promoting the onset of cracks. Additionally, a greater number of voids are present, which also accelerates the hydrogen embrittlement mechanism (H.E.M). Since the number of inclusions in the studied material is very high and initiatory cracks have also been found on the grain boundaries and near inclusions (Subfigure 10 (b)), they could also serve as nucleation points and voids for cracks induced by hydrogen.

Microstructures evolutions

For this, we carried out mechanical polishing and chemical attack with the 10% solution of oxalic acid ($C_2H_2O_4$), including the composition of 10 grams of oxalic acid in 100 millilitres of distilled water with an attack duration of 15 to 40 seconds under a voltage of 6 volts to reveal the microstructures represented in Subfigures 10 (a) and 10 (b) by optical microscopic (OM) reference Leica DM4-GMBH. Subfigure 10 (a) represents the microstructural analysis of the sample in the rough state without heat treatment. It can be seen that the microstructure is composed of several austenite platelets that are homogeneous with each other, with the total absence of precipitates, carbides, inclusions and microcavities. The corresponding microstructures, as Subfigure 10 (b) and Subfigure 11 (b) show, in the condition of austenitic and tempered AISI304 steel, followed by hydrogen charging for 13 hours, show a transformation to the martensitic (M) structure composed of several platelets with a lath-like interior bearing a high density of carbide precipitates and inclusions at the grain boundaries. Using the optical microscopy (OM) technique, an observation of the microstructure of the sample pre-loaded with hydrogen for a duration of 13 hours has revealed a dark area on the matrix near the inclusion known as the optical dark area (ODA), commonly referred to as "fish-eye" defect (Subfigure 12 (b)), similarly to the research conducted by (Murakami & Matsunaga, 2006). Based on these observations, it is noted that the growth in the number of ODAs is not attributed to the application of mechanical fracture solicitations by tensile loading but rather induced by the effect of the high mobility and rapid propagation of diffusible hydrogen (H) localized within interstitial sites, and microstructural defects trapped along the ODA-included zone.

On the other hand, the number of inclusions, as defects, is consistently incoherent with the matrix and serves as high-energy trapping

sites. In the regions where there were few inclusions, hydrogen appeared to weaken the grain boundaries, particularly at the interface between inclusions and the matrix. That led to embrittlement of the studied material without a change in the rupture mode, which continued to be ductile. The same evolution observed by scanning electron microscopy (SEM) (Subfigure 11 (b)) shows a high density and different sizes of ODA zones which are increased and closely spaced among themselves and with carbide precipitates at grain boundaries, depending on the adopted industrial conditions that promote hydrogen loading: the aggressive environment containing dihydrogen, a high density of the applied current, and the hydrogen content diffused with respect to loading durations in hours.

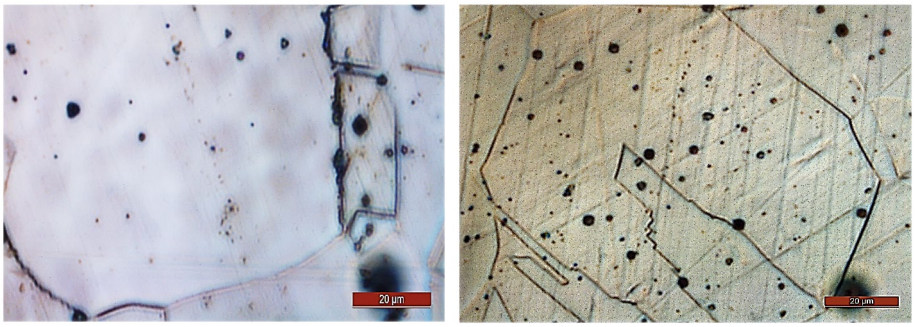

(a) (b)

Figure 10 – (a) Optical microscope (OM) images of the rough microstructure of the stainless steel studied (x20µm), and (b) the microstructure of the AISI304 steel pre-loaded with hydrogen, presented around ODA inclusions and a large density of carbide precipitates, small and medium-sized (x20µm).

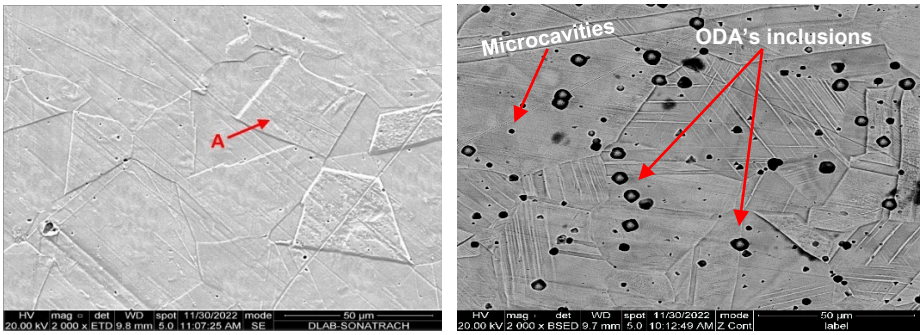

(a) (b)

Figure 11 – (a) Scanning electron microscope (SEM) image of the rough microstructure of AISI304 austenitic stainless steel (x50μm), and (b) the optical dark areas of steel loaded with hydrogen presented around ODA inclusions (fish eye), microcavities and large carbide precipitates in the grain boundaries (x50μm)

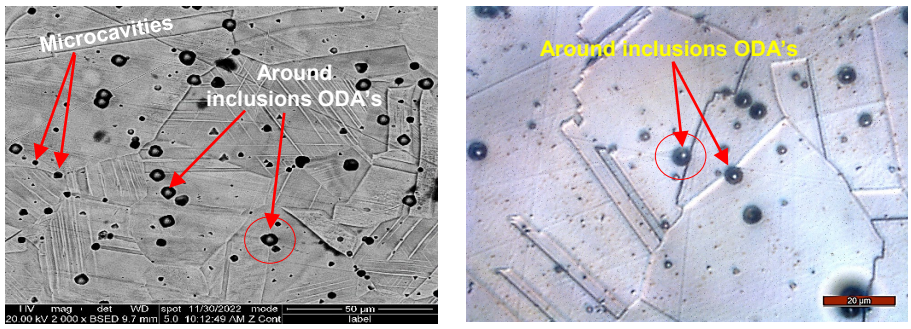

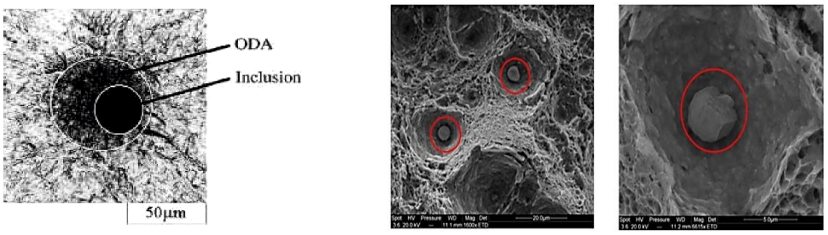

Figure 12 – (a) Scanning electron microscope (SEM) image of the optical dark areas (ODAs) of the AISI304 steel pre-loaded with hydrogen for 13hours, presents micro-cavities and the ODAs around the inclusions (fish eye) (x50μm). (b) The optical microscope (OM) image of the AISI304 steel pre-loaded with hydrogen for 13 hours presents the ODAs around the inclusions (fish eye) (x20μm). (c) The optical micrograph of the fracture origin (JIS SCM435, σ = 561 MPa, Nf = 1.1x10^8) with the optical dark area (ODA) around the inclusion. (Murakami et al., 2006) (x50μm). (d) and (e) The scanning electron microscope (SEM) image of the inclusions in the QTM9 alloy (Murakami et al., 2013) (x20 μm) and (x5 μm)

Under the influence of deformation constraints, the hydrogen pre-loaded into the studied material, as a function of loading durations in hours, will be transported by dislocations to the area of maximum stress plasticity. The accumulation of hydrogen in defects leads to the formation of cracks. The formation of molecules along a row of adjacent hydrogen atoms causes the anchoring of dislocations. At the same time, a fragile zone is

created, where maximum stress develops, reducing the resistance to rupture of the zone and leading to the creation of micro-cracks (Lo et al., 2009). The coalescence of these micro-cracks under the effect of high pressure from hydrogen molecules into a large crack causes the displacement and advancement of this crack. Carbide precipitations at grain boundaries (Lee & Lee, 1987; Aurélie Laureys et al., 2020) or the presence of high-density carbides in various forms of carbide precipitates (Laureys et al., 2018), due to the penetration of the hydrogen molecule (H_2), form which is called a "fish eye" defect, as Subfigure 11 (b), Subfigure 12 (a) and Subfigure 12 (b) show, validated by the work of (Murakami & Matsunaga, 2006), as Subfigures 12 (c), 2 (d), and (e) show (Murakami et al., 2013). In parallel, these small coherent and/or semi-coherent precipitates are associated with low-energy traps. However, they can trap a large amount of hydrogen, while incoherent precipitates are associated with high-energy traps that trap very little hydrogen (Subfigure 10 (b)) (Frappart et al., 2011).

Scanning electron microscope (SEM) analysis

A reference Scanning Electron Microscopy (SEM) Quanta FEG650 (accelerating voltage at 20.00Kv, spot size of 5.0nm) in combination with Energy Dispersive X-ray Analysis (EDXA), for the observation of fracture surfaces on cylindrical specimens, has revealed large inclusionary zones where the number of these inclusions represents privileged sites for the initiation of internal cracks in the mechanism of hydrogen-induced cracking (HIC) (Jin et al., 2010). That is particularly true for the HIC phenomenon. The nature of these ODA (Optical Dark Area) inclusions (Jin et al., 2010) is characterized by their shapes, sizes, numbers, and distribution state, which are their main characteristics. These characteristics have a significant influence on the cracking process in the presence of hydrogen molecules (H_2). The most harmful inclusions are coarse and closely spaced elongated inclusions (Murakami et al., 2013), as shown in Subfigures 12 (a) and (b). This results in a fracture surface where the metallic matrix is less ductile, and micro-cavities that appear at the particle interfaces can act as internal cracks. If the stress intensity factor exceeds the toughness of the material under study, crack propagation then leads to sudden fracture, which is highly brittle, as depicted in Subfigure 9 (b).

The ODAs around the inclusions observed in Subfigure 10 (b) and Subfigure 11 (b) play a significant role in the damage to the studied material. Indeed, the deformation incompatibility between the inclusions and the matrix can lead to local stresses that favour either inclusion fracture or interface decohesion. If the metallic matrix surrounding the

inclusions is ductile, the microcavities created during plastic deformation subsequently grow and ultimately lead to final fracture, typically through the process of coalescence, as depicted in Subfigure 12 (c) (Murakami & Matsunaga, 2006).

In this case, it can be concluded that the influence of hydrogen loading of AISI304 material is indeed significant for tensile rupture, especially when the surface of the fracture face of the sample, quenched/tempered and subsequently loaded for a prolonged duration of 13 hours, exhibits numerous internal cracks in all directions (Subfigure 9 (b)). In parallel, the microstructure matrix observed by SEM represents zones formed by several microcavity holes (Subfigure 11 (b)). This is where carbide precipitates at grain boundaries come into play, exerting their effects by accelerating hydrogen trapping.

The SEM ODA observation represents an intelligent quantitative analysis of the elemental composition of the material studied by EDAX, showing significant changes following the thermal treatments applied and the hydrogen loading process. A significant reduction in the percentages of the key elements is observed compared to the unloaded specimen (in as-delivered condition). Specifically, the carbon content is 6.46% by weight, iron 60.14% by weight, nickel 6.31% by weight, chromium 15.22% by weight, and sulphur 0.76% by weight. In addition, the typical spectral analysis representing the characteristic peaks of the identified elements of a sample preloaded with hydrogen shows the total absence of the elements of aluminium and molybdenum in this treated material. These results are supported by visual representations of the data in Figures 13 and 14, and the reference tables, Tables 4 and 5 in particular. Overall, the results show a significant change in the elemental composition of the material as a result of the electrolytic loading process under the industrial conditions adopted.

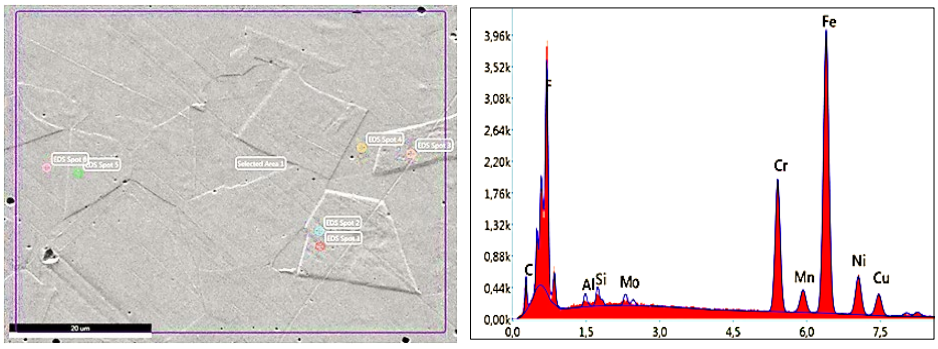

(a) (b)

Figure 13 – (a) Scanning electron microscope (SEM) microstructure (as-delivered condition) of AISI304 stainless steel (x20µm); and (b) Energy-Dispersive X-ray Analysis (EDXA) microanalysis of the elemental composition of AISI304 steel in crude state

Intelligent quantitative results before electrochemically-induced hydrogen loading

The data presented in Table 4 summarise the intelligent quantitative results, expressed in weight percent (%). These results were obtained under as-delivered conditions prior to the implementation of electrochemically induced hydrogen conditions.

Table 4 – Intelligent quantitative results of AISI304 in crude state before electrochemical hydrogen loading

Intelligent quantitative results				
Element	**% mass**	**% atomic**	**Total Intensity**	**Error %**
C K	7.64	25.67	121.29	12.75
F K	4.19	8.89	278.13	11.33
AlK	0.58	0.87	51.09	15.74
SiK	0.69	0.99	82.02	10.66
MoK	0.46	0.57	61.86	12.37
CrK	16.08	12.47	1491.38	3.55
MnK	1.42	1.04	101.55	10.10
FeK	61.71	44.56	3694.93	2.47
NiK	6.53	4.49	286.49	5.34
CuK	0.70	0.44	25.35	22.95

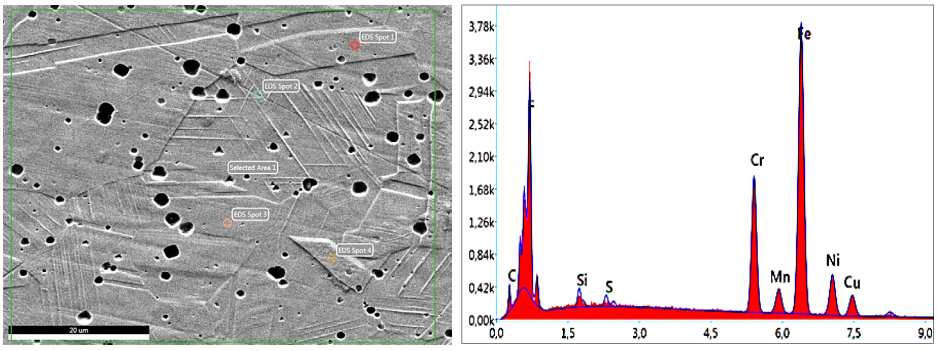

(a) (b)

Figure 14 – (a) Scanning electron microscope (SEM) image of the microstructure of the AISI304 stainless steel specimen after 13 hours of electrochemical hydrogen charging (x20μm), and (b) Energy-Dispersive X-ray Analysis (EDXA) microanalysis indicating the ODAs around the inclusions contained in AISI304 steel

Intelligent quantitative results after electrochemical hydrogen preloading

The initial Intelligent quantitative results expressed in wt (%) of the matrix composition after electrochemical hydrogen preloading are detailed in Table 5.

Table 5 – Intelligent quantitative results in wt (%) after hydrogen preloading

Intelligent quantitative results				
Element	**% mass**	**% atomic**	**Total Intensity**	**Error %**
C K	6.46	22.39	93.18	13.07
F K	4.38	9.82	272.59	11.30
SiK	0.66	0.98	71.44	11.39
S K	0.76	0.66	62.76	12.30
CrK	15.22	12.99	1371.09	3.58
MnK	1.22	1.15	98.95	10.64
FeK	60.14	47.07	3436.50	2.48
NiK	6.31	4.51	252.83	5.70
CuK	0.65	0.43	21.6	29.69

The analysis of Figures 13 and 14 reveals a significant result concerning the presence of sulphur in the materials examined. Specifically, the raw structure shows no sulphur content, whereas the ODA microanalysis indicates the emergence of sulphur (S).

This presence of sulphur is critical because it can react with hydrogen to produce hydrogen sulphide (H_2S). The formation of H_2S is linked to the development of hydrogen embrittlement (HE) in AISI304 stainless steel. Consequently, sulphur is identified as a harmful element that adversely affects the material's resistance to hydrogen embrittlement, highlighting its detrimental impact on the integrity of the steel.

Conclusion

This experimental study investigates the influence of hydrogen induced by the electrochemically-hydrogen preloading process on AISI304 stainless steel ductility, tensile strength, and fracture behavior. Based on the experimental results and analysis using optical microscopy (OM), X-ray diffraction (XRD), and scanning electron microscopy (SEM), the conclusions are drawn as follows:

The variation in the mechanical stress strength (Rm), yield (Re), and failure (Rr) of AISI304 austenitic stainless steel decreases significantly with the increase in the duration time in hours of hydrogen preloading. That can be explained by the fact that hydrogen, diffusing into the atomic lattice of the steel in the form (H), causes weakening of the metallic bond which causes the resistance to decrease until the material breaks.

The increase in the tempering temperature leads to a decrease in the variation in mechanical strength: (Rm), (Re) and the (Rr) with an increase in ductility A (%), Z (%).

The effects caused by the hydrogen embrittlement (HE) phenomenon on AISI304 stainless steel are characterized by a decrease in its ductility, which sometimes undergoes a sudden embrittlement.

Heat treatments and electrolytic hydrogen charging can significantly improve the plasticity of AISI304 austenitic stainless steel.

In cathodic loading, the conditions involved (charging time in hours, high current density, high acid concentration) can lead to a substantial difference in hydrogen concentration between the surface and the core of the internal matrix structure.

All second-phase particles (γ) residual, carbide precipitates, inclusions of small, medium, or large size, as well as interfaces and interphases, can be considered as inclusions. Their mechanical properties and hydrogen transport and segregation mechanisms differ from those of the matrix, particularly in the case where the structure is martensitic. That can be explained by the fact that hydrogen diffusing into steel creates a pseudo-martensitic transformation.

Optical Dark Areas(ODAs) surrounding inclusions manifest as black spots, corresponding to regions of hydrogen accumulation either in the molecular form (H_2) or combined with sulphur in the form H_2S. These two gases are responsible for the HE phenomenon in AISI304 austenitic stainless steel.

Symbols and abbreviations

Rm: Tensile strength, [TS], (MPa)

Re: Yield strength, [YS], (MPa)
Rr: Failure strength, [FS], (MPa)
A: Percentage elongations, in (%)
Z: Percentage reduction, (striction), in (%)
HRV (30): Hardness vickers, in (N/mm^2)
ε̇: Nominal speed, in (mm/min)
E: Young's modulus, in (MPa)
υ: Poisson's modulus
γ: Austenitic phase (A)
α: Ferritic phase (F)
M: Martensitic structure (M)
A : Austenitic structure
ODA: Optical dark area

References

Amar, A. 2023. The Effect of cryogenic heat treatments on the mechanical behavior of hydrogen filled steels. *International Journal of Advanced Sicentific Research and Innovation (IJASRI) Egypt.* Available at: https://www.academia.edu/121805278/The_Effect_of_cryogenic_heat_treatments_on_the_mechanical_behavior_of_hydrogen_filled_steels [11 August 2024].

Amar Abboub, Ahmed Aboura, Khaled Benmahdi, Mohamed Sadoun, Mokhtar Belkacem, Djameleddine Semsoum, "Mechanical behaviour of austenitic stainless steel loaded in the aqueous solution of H2SO4 during tensile testing", *Vojnotehnički glasnik/Military Technical Courier*, 2024, Vol. 72, Issus 4, P.P 1992-2011, Available at: https://doi.org/10.5937/vojtehg72-49964

Aurélie Laureys, Margot Pinson, Lisa Claeys, Tim Deseranno, Tom Depover, & Kim Verbeken. 2020. Initiation of hydrogen induced cracks at secondary phase particles. *Frattura ed Integrità Strutturale*, 14(52): 113–127. Available at: https://www.fracturae.com/index.php/fis/article/view/2710 [8 August 2024].

Bach, A.-C. 2018. *Etude du piégeage de l'hydrogène dans un acier inoxydable austénitique dans le cadre de la corrosion sous contrainte assistée par l'irradiation*.

BARRALIS, J., CASTEX, L. & MAEDER, G. 1999. Précontraintes et traitements superficiels. *Précontraintes et traitements superficiels*, MD1(M1180): M1180.1 (51).

Bhadeshia, H.K.D.H. & Honeycombe, R.W.K. 2006. *Steels: microstructure and properties*. 3rd ed. Amsterdam ; Boston: Elsevier, Butterworth-Heinemann.

Blanchard, R., Pelissier, J. & Pluchery, M. 1960. Effets de l'hydrogene sur les caracteristiques de rupture par traction d'aciers inoxydables. *Journal of Nuclear Materials*, 2(3): 216–224. Available at: https://www.sciencedirect.com/science/article/pii/0022311560900568 [8 August 2024].

Brass, A.-M., Chêne, J. & Coudreuse, L. 2000. Fragilisation des aciers par l'hydrogène : étude et prévention. *Corrosion Vieillissement*. Available at: https://www.techniques-ingenieur.fr/doi/10.51257/a/v2/m175 [9 July 2024].

Cauwels, M., Claeys, L., Depover, T. & Verbeken, K. 2019. The hydrogen embrittlement sensitivity of duplex stainless steel with different phase fractions evaluated by in-situ mechanical testing. *Frattura ed Integrità Strutturale*, 14(51): 449–458. Available at: https://www.fracturae.com/index.php/fis/article/view/2666 [8 August 2024].

Chêne, J. 2009. L'hydrogène dans les matériaux métalliques en relation avec les interactions plasticité-environnement. In *PlastOx 2007 - Mécanismes et Mécanique des Interactions Plasticité - Environnement*. PlastOx 2007 - Mécanismes et Mécanique des Interactions Plasticité - Environnement. Argelès-sur-Mer, France: EDP Sciences: 131–145. http://plastox.edpsciences.org/10.1051/ptox/2009010 [9 July 2024].

Colombié, M. 2008. *Matériaux métalliques*. 2e éd. Paris: Dunod.

Creus, P.J. 2013 DIFFUSION AND SEGREGATION OF HYDROGEN IN MARTENSITIC AISI 5135 : INFLUENCE OF BAKING TIME AT 20°C ON THE HYDROGEN DISTRIBUTION AND EMBRITTLEMENT.

Cunat, P.-J. 2000. Aciers inoxydables - Propriétés. Résistance à la corrosion. *Étude et propriétés des métaux*. Available at: https://www.techniques-ingenieur.fr/doi/10.51257/a/v1/m4541 [8 August 2024].

Depover, T., Pérez Escobar, D., Wallaert, E., Zermout, Z. & Verbeken, K. 2014. Effect of hydrogen charging on the mechanical properties of advanced high strength steels. *International Journal of Hydrogen Energy*, 39(9): 4647–4656. Available at: https://www.sciencedirect.com/science/article/pii/S0360319913031820 [10 July 2024].

DIN TASCHENBUCH 19. 1975. DIN-Taschenbuch 19. Materialprüfnormen für metallische Werkstoffe 1. Available at: https://www.ingenieur-buch.de/din-taschenbuch-19-materialprufnormen-fur-metallische-werkstoffe-1.html [10 July 2024].

El Hilali, F., Habashi, M. & Mohsine, A. 1999. Comportement mécanique de l'acier inoxydable martensitique 17-4 PH en corrosion sous contrainte et à la fragilisation par l'hydrogéne environnemental. *Annales de Chimie Science des Matériaux*, 24(3): 169–194. Available at: https://www.sciencedirect.com/science/article/pii/S0151910799800440 [9 August 2024].

Frappart, S., Oudriss, A., Feaugas, X., Creus, J., Bouhattate, J., Thébault, F., Delattre, L. & Marchebois, H. 2011. Hydrogen trapping in martensitic steel investigated using electrochemical permeation and thermal desorption spectroscopy. *Scripta Materialia*, 65(10): 859–862. Available at: https://linkinghub.elsevier.com/retrieve/pii/S1359646211004416 [8 August 2024].

Grimault, B., Chauveau, E., Gaillet, L., Drissi-Habti, M., Chaussadent, T. & Mantel, M. 2012. Comportement d'aciers inoxydables à hautes caractéristiques mécaniques vis-à-vis de la corrosion par piqûre et de la fragilisation par

hydrogène. *Matériaux & Techniques*, 100(2): 113–125. http://www.mattech-journal.org/10.1051/mattech/2012008 [9 July 2024].

Hamissi, C., Lakhdari, A., Aboura, A. & Seddak, M. 2016. Hydrogénation des vis en acier 35B2 lors du décapage acide. *Revue des matériaux et énergies renouvelables*, 1(1): 1–7. Available at: https://www.asjp.cerist.dz/en/article/67672 [9 August 2024].

He, J., Han, G., Fukuyama, S. & Yokogawa, K. 1999. Tensile behaviour of duplex stainless steel at low temperatures. *Materials Science and Technology*, 15(8): 909–920. Available at: https://journals.sagepub.com/doi/full/10.1179/026708399101506715 [9 July 2024].

Iacoviello, F. 1995. V - Fragilisation par l'hydrogène de l'acier inoxydable duplex Z2CND2205 chargé en hydrogène à 200°C. *Matériaux & Techniques*, 83: 48–50. http://www.mattech-journal.org/10.1051/mattech/199583120048s [9 July 2024].

Jin, T.Y., Liu, Z.Y. & Cheng, Y.F. 2010. Effect of non-metallic inclusions on hydrogen-induced cracking of API5L X100 steel. *International Journal of Hydrogen Energy*, 35(15): 8014–8021. Available at: https://linkinghub.elsevier.com/retrieve/pii/S0360319910010591 [27 December 2024].

Laureys, A., Claeys, L., De Seranno, T., Depover, T., Van Den Eeckhout, E., Petrov, R. & Verbeken, K. 2018. The role of titanium and vanadium based precipitates on hydrogen induced degradation of ferritic materials. *Materials Characterization*, 144: 22–34. Available at: https://linkinghub.elsevier.com/retrieve/pii/S1044580318310386 [8 August 2024].

Lee, J.-L. & Lee, J.-Y. 1987. The effect of lattice defects induced by cathodic hydrogen charging on the apparent diffusivity of hydrogen in pure iron. *Journal of Materials Science*, 22(11): 3939–3948. http://link.springer.com/10.1007/BF01133343 [8 August 2024].

Lo, K.H., Shek, C.H. & Lai, J.K.L. 2009. Recent developments in stainless steels. *Materials Science and Engineering: R: Reports*, 65(4–6): 39–104. Available at: https://linkinghub.elsevier.com/retrieve/pii/S0927796X09000461 [8 August 2024].

Ly, C. 2009. *Caractérisation d'aciers à très haute limite d'élasticité vis-à-vis de la fragilisation par l'hydrogène*.

Lynch, S. 2012. Hydrogen embrittlement phenomena and mechanisms. *Corrosion Reviews*, 30(3–4). Available at: https://www.degruyter.com/document/doi/10.1515/corrrev-2012-0502/html [8 August 2024].

Murakami, Y., Kanezaki, T. & Sofronis, P. 2013. Hydrogen embrittlement of high strength steels: Determination of the threshold stress intensity for small cracks nucleating at nonmetallic inclusions. *Engineering Fracture Mechanics*, 97: 227–243. Available at: https://linkinghub.elsevier.com/retrieve/pii/S0013794412004377 [8 August 2024].

Murakami, Y. & Matsunaga, H. 2006. The effect of hydrogen on fatigue properties of steels used for fuel cell system. *International Journal of Fatigue*, 28(11): 1509–1520. Available at: https://linkinghub.elsevier.com/retrieve/pii/S0142112306001009 [8 August 2024].

Na Li, Wei Wang, Qimin liang, Effect of hydrogen embritllement and non-metallic inclusions on tensile fracture properties of 55CrSi spring steel, Mater, Res. Express 7 046520. Available at: https://iopscience.iop.org/article/10.1088/2053-1591/ab8b19/pdf

Prieto, G. & Tuckart, W.R. 2017. Influence of Cryogenic Treatments on the Wear Behavior of AISI 420 Martensitic Stainless Steel. *Journal of Materials Engineering and Performance*, 26(11): 5262–5271. http://link.springer.com/10.1007/s11665-017-2986-y [8 August 2024].

Pundt A. & Kirchheim R., Hydrogen in metals : Microstructural aspects, Annu. Rev. Mater. Res. 36, 555–608, 2006. Available at: https://doi.org/10.1146/ANNUREV.MATSCI.36.090804.094451

Robertson, I.M., Sofronis, P., Nagao, A., Martin, M.L., Wang, S., Gross, D.W. & Nygren, K.E. 2015. Hydrogen Embrittlement Understood. *Metallurgical and Materials Transactions A*, 46(6): 2323–2341. Available at: https://link.springer.com/10.1007/s11661-015-2836-1 [9 July 2024].

Sales, D.G. 2015. *Etude des mécanismes d'endommagement d'aciers martensitiques associés au SSC (Sulphide Stress Cracking)*. Available at: https://theses.hal.science/tel-03091976

.

Утицај електролитичког оптерећења водоником на механичка својства и микроструктуру аустенитног нерђајућег челика AISI 304

Амар Абуба[а], **аутор за преписку**, *Ахмед*Абура [б], *Халед Бенмахди*[а], *Мохамед* Садун[а], *Мохамед* Букелеф[а]
[а] Универзитет Мустафа Стамбули, Факултет наука и технологије, Одсек за машинство, Маскара, Народна Демократска Република Алжир,
[б] Универзитет Ахмед Забана, Факултет наука и технологије ,

ОБЛАСТ:материјали
КАТЕГОРИЈА (ТИП) ЧЛАНКА: оригинални научни рад

Сажетак:

Увод/циљ: Водонична кртост (HE) у знатној мери умањује механичка својства аустенитних нерђајућих челика чиме ограничава њихову ефикасност у различитим применама. У раду се испитује утицај изложености електролитичком водонику на механичке карактеристике и микроструктуру широко заступљеног аустенитног нерђајућег челика AISI 304.

Методе: Затезне епрувете пречника 8 мм произведене су машинском обрадом и подвргнуте оптерећењу електролитичким водоником у различитом трајању у стакленој комори са 0,05 M

сумпорне киселине (H_2SO_4). Механичка испитивања су вршена на кидалици универзалног типа 83431 фирме „Карл Франк GmbH". Епрувете су микроскопски испитане помоћу оптичког микроскопа (OM), дифракције X зрака (XRD) и скенирајуће електронске микроскопије (SEM). У процесу експерименталне карактеризације израђене су цилиндричне епрувете које су затим подвргнуте термичкој обради (аустенизацији), од каљења до отпуштања, као и циклусу накнадне изложености хладноћи на -196°C у трајању од 35 минута.

Предоптерећење водоником изведено је електрохемијским путем – за различита времена оптерећења у сатима.

Резултати: Резултати су показали да се утицај водоничне кртости на нерђајући челик AISI 304 огледа у смањењу дуктилности и понекад у наглој кртости. Ова појава је конзистентно уочена и у радовима других аутора који су указали на губитак дуктилности услед мартензитне трансформације аустенита проузроковане деформацијом и дифузијом водоника.

Закључак: Честице друге фазе – карбидни преципитати, инклузије малих, средњих или великих димензија, интерфејсови и међуфазе могу се сматрати инклузијама. Њихова механичка својства и транспорт водоника, као и механизми сегрегације, разликују се од оних који одликују матрицу, нарочито у мартензитним структурама. Уочавање оптички тамне области (optical dark area – ODA) и црних тачака указује на то да је водоник концентрисан или у молекуларном облику H_2 или комбинован са сумпором у облику H_2S.

Кључне речи: нерђајући челик AISI 304, термичка обрада, механичка својства, оптерећење водоником, водонична кртост, микроструктура

Paper received on: 16.01.2025.
Manuscript corrections submitted on:06.05.2025.
Paper accepted for publishing on: 27.05.2025.